New insights into the mechanism of photodegradation of chitosan

Pierre-Olivier Bussiere, Jean-Luc Gardette, Géraldine Rapp, Claire Masson, Sandrine Therias

New insights into the mechanism of photodegradation of chitosan

Pierre-Olivier Bussière, Jean-Luc Gardette
Géraldine Rapp, Claire Masson and Sandrine Therias*
Université Clermont Auvergne, CNRS, SIGMA Clermont, ICCF
F-63000 Clermont-Ferrand, France

Abstract

(150 words)

Chitosan films were subjected to accelerated artificial weathering at $\lambda > 300$ nm and 60°C in the presence of O_2. The resulting variations in the chemical structure were characterized by IR spectroscopy and UV-visible spectroscopy, and a photooxidation mechanism was proposed based on the identified oxidation photoproducts. The formation of gluconolactone derivatives leading to chain scissions was shown. In addition, low molecular weight photoproducts, which accounted for chitosan deacetylation, were detected. Furthermore, crosslinking reactions occurred, as revealed by gel fraction characterization. Variations in the mechanical and surface properties were characterized by AFM, and the reduction in macroscopic properties was correlated with the structural changes observed at the molecular scale by a multiscale approach.

Keywords: chitosan; photodegradation; oxidation; mechanism

*Corresponding author:

E-mail addresses: pierre-olivier.bussiere@sigma-clermont.fr (P.O. Bussiere), luc.gardette@uca.fr (J.L. Gardette), geraldine.rapp@uca.fr (G. Rapp), claire.poncet@uca.fr (C. Masson), sandrine.therias@uca.fr (S. Therias)

1. Introduction

Chitosan is a natural polysaccharide composed of N-acetyl glucosamine and glucosamine units, two derivatives of glucose, that are linked together by glycosidic bonds (Synytsya, Grafova, Slepicka, Gedeon & Synytsya, 2012) (Scheme 1). The presence of hydroxyl and amino groups promotes H bonds between macromolecular chains. Thus, chitosan can crystallize into a hydrated form and an anhydrous form (Ogawa, Yui & Okuyama, 2004). Due to its solubility in water, biodegradability, biocompatibility and non-toxicity, many studies have focused on the use of chitosan for medical purposes such as soft tissue engineering (Tchemtchoua et al., 2011), bone tissue engineering (Nazeer, Yilgor, Yilgor, 2017) and drug release (Lien et al., 2012). Due to the same "green" characteristics, chitosan was studied to be employed as a scaffold for water treatment (Moczek & Nowakowska, 2007) and as packaging material in the food industry (Aider, 2010).

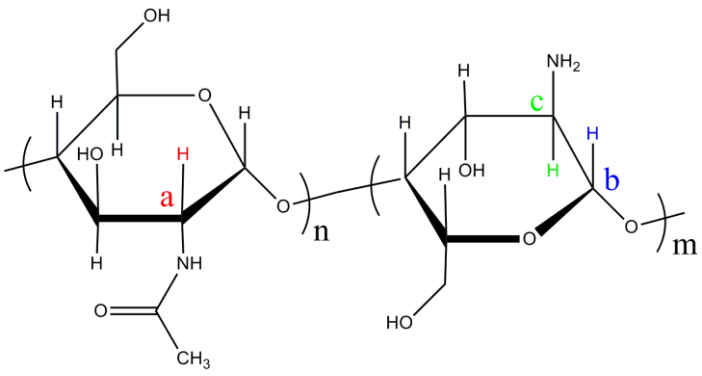

Scheme 1: Chemical structure of chitosan

The dependence of the thermal degradation of chitosan on the degree of deacetylation was studied (Gamiz-Gonzalez et al., 2017), (Villar-Chavero, Dominguez, Alonso, Oliet & Rodriguez, 2018). Changes in the degree of deacetylation of chitosan were reported during thermal treatment above 200°C (Zawadzki &Kaczmarek, 2010). The effect of the degree of deacetylation on the radiation-induced degradation of chitosan (Taskn, Cansag, Sen, 2014) was also investigated and revealed that deacetylation is an important factor for controlling the degradation rate of chitosan. Degradation of chitosan under different stresses (microwave (Wasikiewicz & Yeates, 2013) and cavitation (Huang, Wu, Huang, Yang & Ren, 2013) has also been reported. Regarding photodegradation, a few papers report the use of UV irradiation as a sterilizing agent at a wavelength of 254 nm: chitosan (Sionkowska, Planecka,

Lewandowska, Kaczmarek & Szarszewska, 2013) (Andrady, Torikai, Kobatake, 1996) (Mucha &Pawlak, 2002); blends of chitosan/poly(vinyl pyrrolidone) (Sionkowska, Wisniewski, Skopinska, Vicini & Marsano, 2005) and of chitosan/poly(ethylene oxide) (Kowalonek, 2017); and chitosan modified with keratin (Sionkowska, Skopinska-Wisniewska, Planecka & Kozlowska, 2010), with silk fibroin (Sionkowska, Planecka, Lewandowska & Michalska, 2014) or with tannic acid (Sionkowska, Kaczmarek, Gnatowska & Kowalonek, 2015). The effect of UV degradation was mainly characterized on the thermal or mechanical properties but also on the surface of chitosan films (Sionkowska, 2006). UV irradiation at λ = 254 nm was shown to provoke a decrease in molecular weight as a result of chain scissions. Changes in IR spectra were observed, such as the formation of bands attributed to carbonyl groups at 1730 cm^{-1} and an increase of bands attributed to amide at 1655 cm^{-1} (C=O) and 1560 cm^{-1} (N-H) accompanied with a decrease of the IR band at 1590 cm^{-1} corresponding to the amine group (Sionkowska et al; 2013) (Mucha &Pawlak, 2002).
One study reports the TiO_2 photocatalytic-oxidation of solid-state chitosan under fluorescent irradiation (Nawi, Jawad, Sabar & Wan Ngah, 2011); more recently, the effect of UV irradiation on the physicochemical characteristics of chitosan modified with nanoparticles of silver vanadate (Abdelghany, Ayaad & Aboelkheir, 2019) was reported. However, weathering of chitosan films under UV-light irradiation at long wavelengths (λ>300 nm) under accelerated conditions of natural outdoor weathering has received little attention (Sionkowska, Planecka, Kozlowska, Skopinska-Wisniewska, Los, 2011), and no mechanism of photooxidation has been proposed.

The aim of this work is to propose a photodegradation mechanism of chitosan in photooxidative conditions at λ > 300 nm under accelerated artificial conditions (at 60°C in the presence of O_2), which can explain the variations in material properties. The main objective of the paper is to provide evidence of the consequences of photochemical reactions on the macroscopic properties of chitosan and to qualitatively and quantitatively confirm the direct relationship between variations in the chemical structure and variations in the mechanical properties due to a multiscale approach of the degradation.

2. Experimental

2.1. Materials

Chitosan was purchased from Polysciences Inc. as a purified powder with an average molecular weight of 15 000 $g.mol^{-1}$ and a minimum degree of deacetylation of 85%. –Thus, the R group in Scheme 1 is defined as –H for 85 % of monomer and as acetamide group for 15 % of monomer. The deacetylation degree of the chitosan film (after Soxhlet treatment) was monitored using IR spectra by following the formula given by Kasaai (Kasaai, 2008) for the ratio of absorbance at 1655 cm^{-1} and 3450 cm^{-1}, at 1320 cm^{-1} and 1420 cm^{-1}, and at 1560 cm^{-1} and 2875 cm^{-1}. The degree of deacetylation was then estimated to be 82 ± 4 %, and the NH_2 group predominated the acetamide group in this chitosan sample.

To prepare the films, chitosan powder was dissolved in acidified water (acetic acid 1% v/v, pH = 5) at a concentration of 10-20 $mg.mL^{-1}$ and stirred for 3 h at 60°C. Solutions were then deposited in Petri dishes, and self-standing films were obtained after drying in ambient air for a few hours. Films of thickness in the range 25 – 50 µm or 150 µm were obtained for the different subsequent analyses. Purification of the films was performed by Soxhlet extraction in MeOH for 24 h. The films were then dried at 60°C under vacuum for 14 hours.

2.2. Irradiation

UV-visible light irradiation (λ > 300 nm) of thin films was performed in a SEPAP 12/24 unit, which was designed for studying polymer photodegradation during artificial ageing with medium-accelerated conditions (Philippart, Sinturel & Gardette, 1997). The chamber consisted of a square reactor equipped with four medium-pressure mercury lamps situated vertically at each corner of the chamber. Wavelengths below 300 nm were filtered by the borosilicate envelope of the lamps, acting as a UV filter below 300 nm (see Fig S1). In the centre of the chamber, the samples were fixed on a 13 cm-diameter rotating carousel that can hold 24 samples. The temperature in the chamber of SEPAP 12/24 is controlled at the surface of a polymer film through a Pt 1000 probe and continually regulated by air circulation. The temperature at the surface of the samples was set to 60°C.

2.3. Characterization Techniques

Spectroscopic analysis

Changes in the UV-visible spectra were monitored with a Shimadzu 2600 plus spectrophotometer equipped with an integrating sphere. IR spectra were recorded in transmission mode with a Nicolet 6700 Fourier transform infrared (FTIR) spectrophotometer operated with OMNIC software. The spectra were obtained with 32 scan summations at 4 cm^{-}

^{1} resolution. IR analysis of chitosan powder was performed by mixing 2 mg of this powder with 200 mg of KBr.

Chemical derivatization reaction

Most of the oxidation products were identified by performing chemical derivatization treatments that selectively convert oxidation products into chemical groups with different IR characteristics (Wilhelm & Gardette, 1994). Ammonia (NH_3) reacts with carboxylic acids to generate carboxylate ions and with esters to generate amides. NH_3 treatment was performed at room temperature in simple flow reactors that could be sealed off to allow the reaction to proceed. 2,4-Dinitrophenylhydrazine (2,4 DNPH) was used to identify aldehydes and ketones. The formation of 2,4-dinitrophenylhydrazone can be detected by two IR absorption bands at 1595 cm^{-1} and 1620 cm^{-1} and a very intense UV-Vis absorption band at 365 nm.

Solid Phase Micro Extraction (SPME)

Films were irradiated in sealed vials to collect the volatile photodegradation products. SPME analysis was performed using Carboxen–PDMS fibres (75 mm) from Supelco (Bellefonte, PA, USA) with an extraction time of 5 min at 60°C, and gas chromatography-mass spectrometry (GC-MS) was performed with a PEG Supelcowax® 10 column (30 m x 0.25 mm x 0.25 mm) from Supelco.

Gel fraction

Crosslinking of polymers was evaluated by gravimetric measurements of the gel fraction (Gf). Irradiated films (approximately 5 mg) were immersed in acidified water (acetic acid 1% v/v) (5 mL) for 48 h. The solutions were then filtered using a Büchner funnel. The insoluble fractions were dried at 60°C and then weighed. The gel fraction is defined by equation 1:

$$Gf = \frac{M_{insoluble}}{M_{initial}} \quad (1)$$

Atomic force microscopy

AFM measurements were performed in tapping mode using an atomic force microscope (AFM) Bruker Multimode driven by a Nanoscope V control unit. The surface topographical images were analysed by the Nanoscope 7.20 software. Images were obtained at three different locations, and the average roughness was determined from these images at four

different locations for each image. The tip was an RTESPA-300 cantilever (Bruker) with a spring constant of approximately 40 N/m and a radius of curvature of approximately 8 nm.

AFM nano-indentation

The force–distance curves were measured at a constant deflection (or constant load). Nano-indentations were performed using a diamond tip (64.05 kHz) with a spring constant of 234.5 N/m and a curvature radius of 25 nm. Three tests of nano-indentation were performed on different areas of the polymer film. Each test corresponded to nine indentations; thus, 3×9 force curves were used with a load that varied from 1 to 5 μN. The force-displacement curves obtained via AFM nano-indentation measurements were analysed using the model proposed by Oliver and Pharr (Oliver & Pharr, 1992) (procedure (O&P)).

AFM nanoscale thermal analysis

Variations in the thermal properties of the films were monitored at the surface using an AFM nanoscale thermal analysis module (Vita). The probe was heated from 20°C to 300°C at a rate of 5 °C/s, and each measurement was performed 3 times to ensure good reproducibility. The Vita probes can also be used to obtain AFM images of the surface (Collin et al., 2012).

3. Results and discussion

3.1. Characterization of chitosan films before irradiation

The main spectral features of chitosan and assignment of the IR bands according to the literature (Mucha & Pawlak (2002)(Valentin, Bonelli, Garrone, Di Renz &, Quignard, 2007) are the OH and NH stretching bands at 3435 cm^{-1} and between 3300-3150 cm^{-1}, respectively, the C=O stretching band at 1655 cm^{-1}, the NH_2 scissoring and NH deformation bands at 1590 cm^{-1} and 1560 cm^{-1} and the C-O-C stretching band attributed to the osidic bond or pyranose ring at 1150 cm^{-1}. Figure 1 compares the carbonyl domain in the IR spectrum of the commercial chitosan powder pressed into a KBr pellet to the same domain in the IR spectra of the pristine films before and after Soxhlet extraction in MeOH for 24 h.

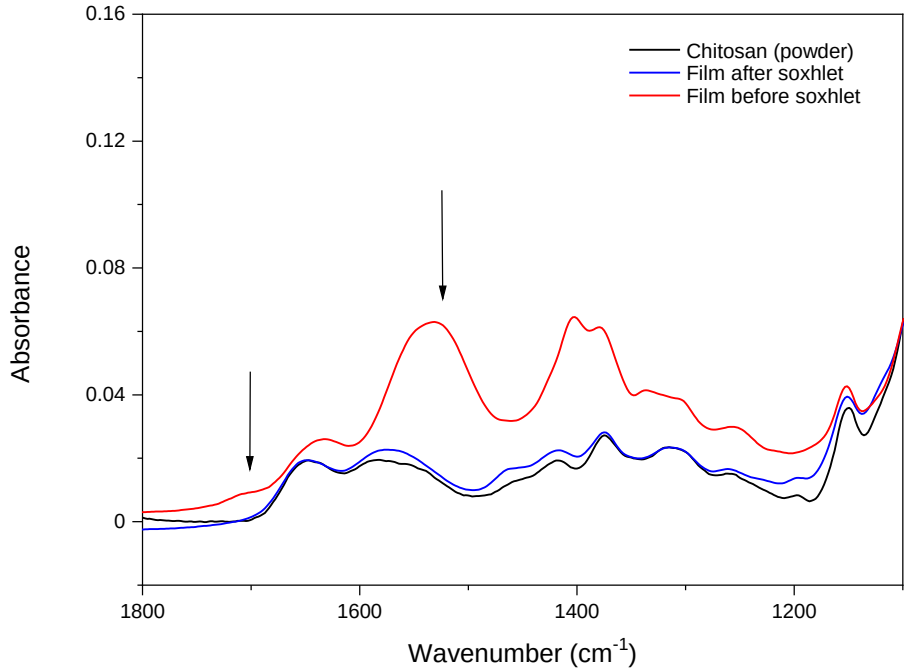

Figure 1: IR spectra of chitosan films (e = 25 µm) before and after 24 h Soxhlet extraction in MeOH and the chitosan powder in KBr pellets.

The IR spectra shown in Figure 1 indicate that Soxhlet extraction of the chitosan film in MeOH provokes the disappearance of three IR bands at 1710 cm^{-1}, 1550 cm^{-1} and 1410 cm^{-1}. This finding can be attributed to the removal of acetic acid and acetate ions. These two products are retained from the process that was used to obtain the films and involved preliminary dissolution in acetic acid-containing solution, which could therefore be trapped within the films at low concentrations even after drying. Acetate ammonium groups are likely generated as a result from the reaction of acetic acid with the amine functions of chitosan (Rinaudo, Pavlov & Desbrieres, 1999). The IR spectrum of chitosan film after Soxhlet extraction is similar to the spectrum of chitosan powder that was pressed into KBr pellets. The experiments reported in this paper were performed for chitosan films that were purified by Soxhlet extraction in MeOH for 24 h.

3.2. Photooxidation of chitosan

3.2.1. Analysis of chemical variations by IR spectroscopy

Irradiation in accelerated artificial conditions at $\lambda > 300$ nm in the presence of O_2 (photooxidation) resulted in noticeable modifications to the IR spectra (Figure 2a). Irradiation provoked a marked decrease in the absorption in the domain 3500 – 3300 cm^{-1}, which

indicates a loss of constitutive water or water generated from the dissolution process and/or breaking of hydrogen bonds present in the chitosan film (Ogawa et al., 2004). A decrease in the IR absorption band of C-O-C bonds at 1150 cm^{-1} was also observed, which could reflect chain scission reactions and/or ring opening of glucosamine and N-acetyl glucosamine. To visualize the changes in the IR spectra in the carbonyl domain, the spectra were subtracted from those of the unexposed film in the domain 2000-1500 cm^{-1} and are presented in Figure 2b. A relatively broad band was observed, with a maximum at 1675 cm^{-1} and shoulders at 1730 cm^{-} and 1780 cm^{-1}. This result is similar to the 254 nm irradiation-induced spectral variations reported in the literature, which proposed chain scission reactions and cleavage of glycosidic bonds (Andrady et al. 1996) (Mucha & Pawlak, 2002) (Wasikiewicz, Yoshii, Nagasawa, Wach & Mitomo, 2005) (Wang, Huang & Wang, 2005).

a)

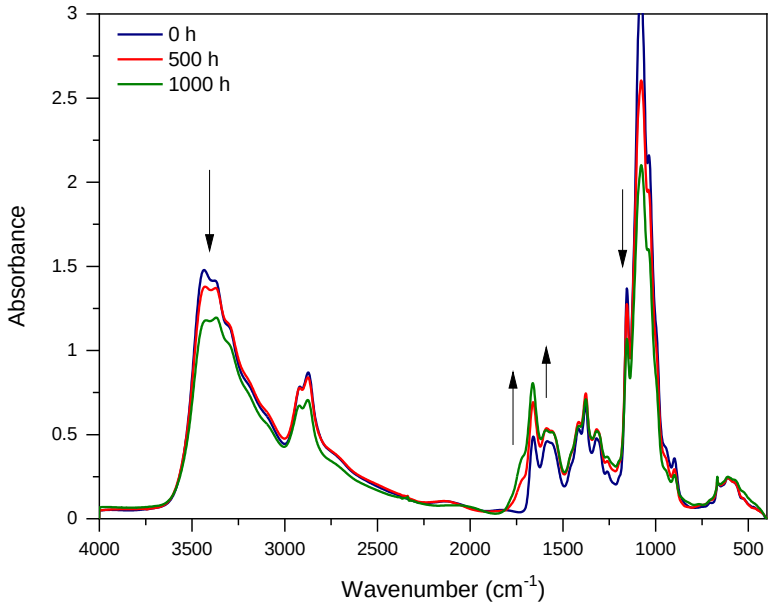

b)

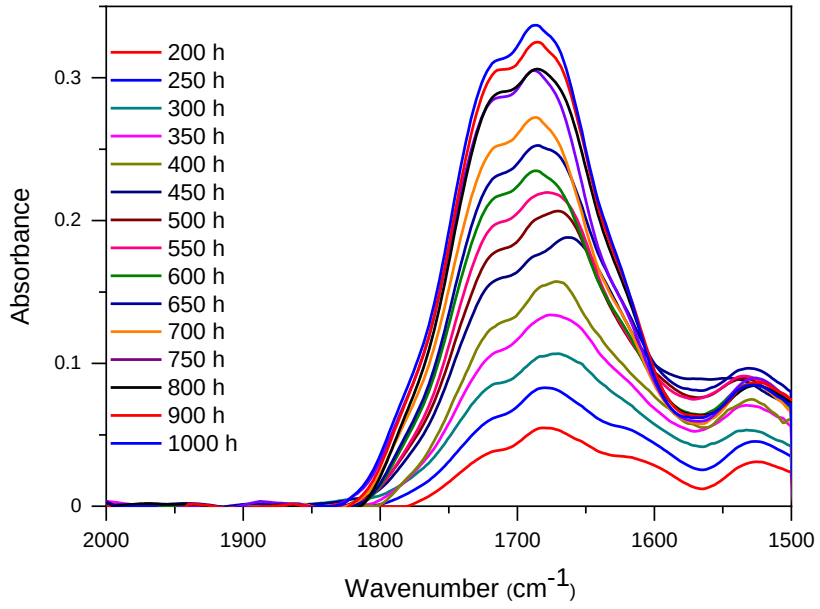

Figure 2: a) IR spectra of a chitosan film (e = 25 µm) during photooxidation
b) Subtracted IR spectra in the carbonyl domain

The decrease in absorbance at 1150 cm^{-1} (Figure 2) reflects the disappearance of the pyranose ring/acetal bond and can be correlated with the accumulation of oxidation products at 1730 cm^{-1}. As proposed by several authors (Mucha & Pawlak, 2002) (Sionkowska, 2011), the accumulation of oxidation products at 1730 cm^{-1} could be related to the formation of an ester function and simultaneous disappearance of the β–1,4 osidic bond. Taking into account the correlation between the increase in absorbance at 1730 cm^{-1} and the decrease at 1150 cm^{-1}, which reflects the disappearance of the pyranose ring/acetal bond (hydrogen abstraction on carbon atom (b) in Scheme 2), this ester bond formation would be consistent with the generation of gluconolactone.

The IR band at 1675 cm^{-1} can be attributed to the vibration νC=O of a carbonyl function of amide I. Considering the chemical structure of chitosan, the formation of a primary amide can also be explained by a mechanism involving oxidation in the α– position of the amine function (hydrogen abstraction on carbon atom (c)). This mechanism is represented in Scheme 2 and discussed at a later point in the manuscript.

3.2.2. Derivatization treatment

Chemical derivatization treatments with NH_3 were performed to identify the degradation products observed by IR analysis at 1730 cm^{-1}. NH_3 reacts with carboxylic acids to generate carboxylate ions and reacts with esters, lactones and anhydrides to generate amides. First, it was verified that no reaction with NH_3 occurred with pristine chitosan. NH_3 treatment of photooxidized films provoked a decrease in the broad absorption at 1730 cm^{-1} and the formation of two weak bands at 1640 cm^{-1} and 1595 cm^{-1} (see Fig. S2). These bands indicate the formation of amides (1640 cm^{-1}) and ammonium carboxylates (1595 cm^{-1}). Amides were formed from the reaction of NH_3 with esters or anhydride, and ammonium carboxylates resulted from the reaction of NH_3 with carboxylic acid or anhydrides. NH_3 treatment allows the identification of esters and carboxylic acids as oxidation photoproducts.

Ester formation was suggested by several authors (Sionkowska et al., 2013), (Andrady et al., 1996) (Mucha & Pawlak, 2002) (Wasikiewicz et al., 2005), but to the best of our knowledge, direct evidence of gluconolactone formation has not yet been reported. For comparison and to confirm the presence of gluconolactone in the photooxidized chitosan film, molecular gluconolactone was blended with pristine chitosan, and the blend was analysed by IR spectroscopy. The IR spectrum is shown in Figure 3a, which clearly confirms the existence of the absorption band at 1730 cm^{-1} attributed to the ν(C=O) vibration band of gluconolactone.

a)

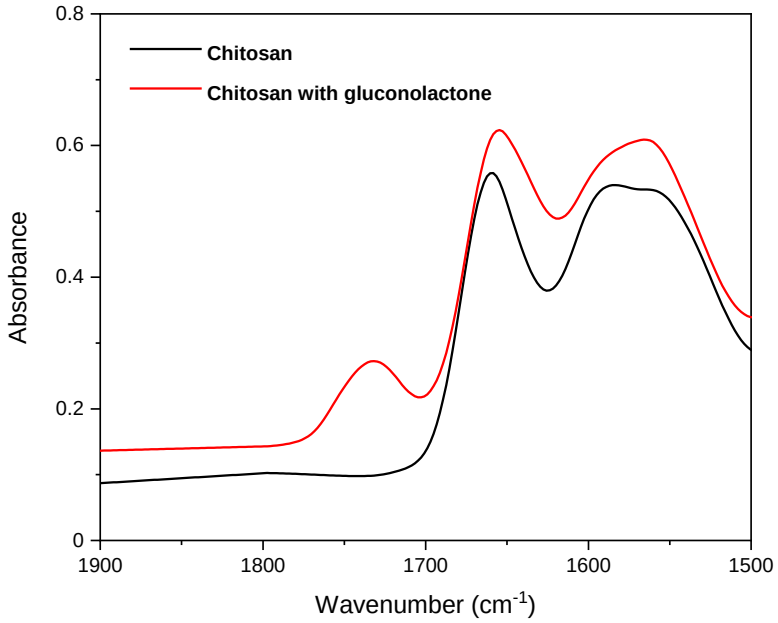

Figure 3a: IR spectrum of a film (e=25 µm) of chitosan blended with gluconolactone.

b)

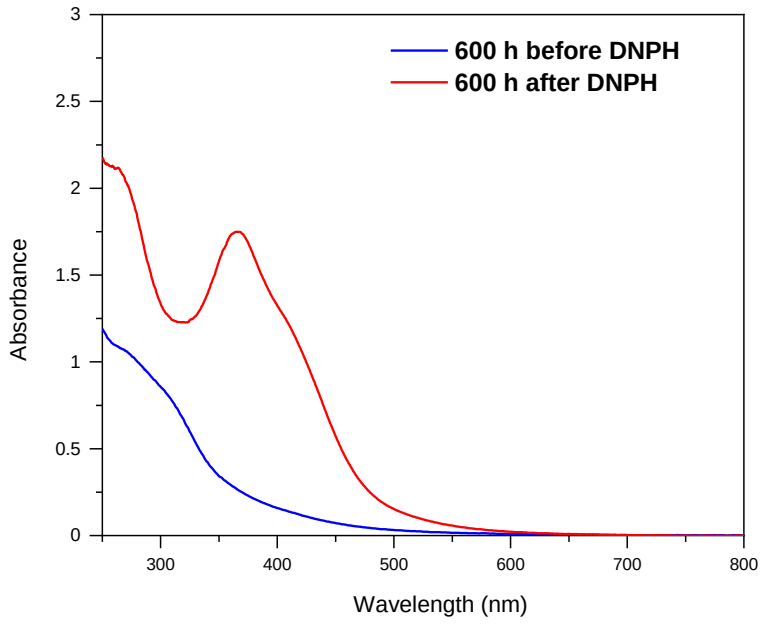

Figure 3b: UV-visible spectra of a 600 h photooxidized chitosan film before and after treatment with 2,4-DNPH.

To complete the identification of the oxidation photoproducts, chemical treatment using 2,4-DNPH was performed on photooxidized chitosan films. The UV-visible spectra of photooxidized chitosan films after 2,4-DNPH treatment (Figure 3b) show a broad band with a maximum at 365 nm corresponding to the phenylhydrazone derivative. This result indicates that aldehydes and/or ketones were formed by the photooxidation of chitosan.

3.2.3. Analysis of volatile products

Photooxidation of polymers is known to be responsible for the formation of low molecular weight products that are likely to migrate from the solid polymer samples and are not detected by the analysis of the films by the spectroscopic methods reported above (Gaume, Wong-Wah-Chung, Rivaton, Therias, Gardette, 2011). To identify the volatile degradation products, SPME-GC/MS was performed. Formamide and acetamide were detected as the main degradation products (see Figure S3). It is also important to note the presence of acetic acid, which was used to solubilize chitosan. As formamide and acetamide molecules contain nitrogen atoms in their structure and therefore are not formed by photooxidation of the cellulose backbone, these products can be attributed to the degradation of the pending groups of chitosan. As a consequence, the deacetylation degree of the chitosan film is changed.

The formation of volatile products (such as acetamide) and the accumulation of ketone/aldehyde groups can be connected to the cleavage of pending groups on carbon atoms (a), following the mechanism given in Scheme 2.

3.2.4. Characterization of chain scission/crosslinking

Gel fraction

To provide evidence of the variations in polymer architecture, the insoluble/gel fractions of photooxidized chitosan films were measured for irradiation times as long as 400 hours. The gel fraction of photooxidized chitosan films increased progressively from 0 (no insoluble fraction before irradiation) to 96 % after 400 hours of irradiation, which indicates that the polymer becomes almost insoluble. This high gel fraction value can be attributed to the formation of a three-dimensional network from crosslinking during the irradiation of chitosan.

3.3 Degradation mechanism

A photooxidation mechanism that explains the formation of the identified photoproducts was proposed (Scheme 2). This mechanism is based on a radical chain reaction with initial hydrogen abstraction on the carbon atoms noted (a), (b) and (c) by radicals from chromophoric impurities, or defects that in commercial chitosan could include proteins and metals. The photodissociation of acetamide groups attached to glucosamine unit, (broad band from 250 till 350 nm) could also be a potential source of radicals able to initiate the chain reaction. However, despite the many articles published in the literature, no real proof was brought that this reaction occurs on exposure to wavelengths above 300 nm. (Rideal & Mitchell, 1937). However, no evidence was obtained that this reaction would occur (Sharkey & Mochel,1959). (Moore, 1963). Radical Oxygenated Species such as HOO·, HO·, R-OO· can be formed and initiate the oxidation by hydrogen abstraction on the polymer chains. The initiation processes in polymer degradation have been reviewed many times in the literature (see for example Scott, 1995). This is followed by the addition of dioxygen, the formation of hydroperoxides and the decomposition of hydroperoxides to generate macroalkoxy radicals (Scheme 2). Hydrogen abstraction from the carbon atom (a) generates the macroalkoxy radical A, which may decompose to generate gluconolactone (its IR band at 1730 cm^{-1} was identified by NH_3 treatment). This reaction generates lactones such as gluconolactone and is accompanied by chain scissions. Hydrogen abstraction from carbon (c) leads to the formation of radical C, which may decompose to form amide groups via ring-opening (IR band at 1675 cm^{-1}).

An important issue is the role played by the temperature in the photooxidation performed at 60°C. Thermal ageing at 60°C in a ventilated oven in absence of light (dark control) during the same time (up to 420 h) was then performed. Comparing the IR spectra after exposure for 420 h to thermooxidation at 60°C or 400 h to photooxidation at $\lambda > 300$ nm-60°C (see Fig. S4) clearly indicates that the IR spectra was only slightly modified after thermooxidation for 420 h, whereas exposure to light at $\lambda > 300$ nm-60°C resulted in dramatic modification of the infrared spectra with the formation of the photproducts which formation has been described above (part 3.2.1). This result clearly indicates that in the current ageing conditions, the oxidation mainly results from irradiation.

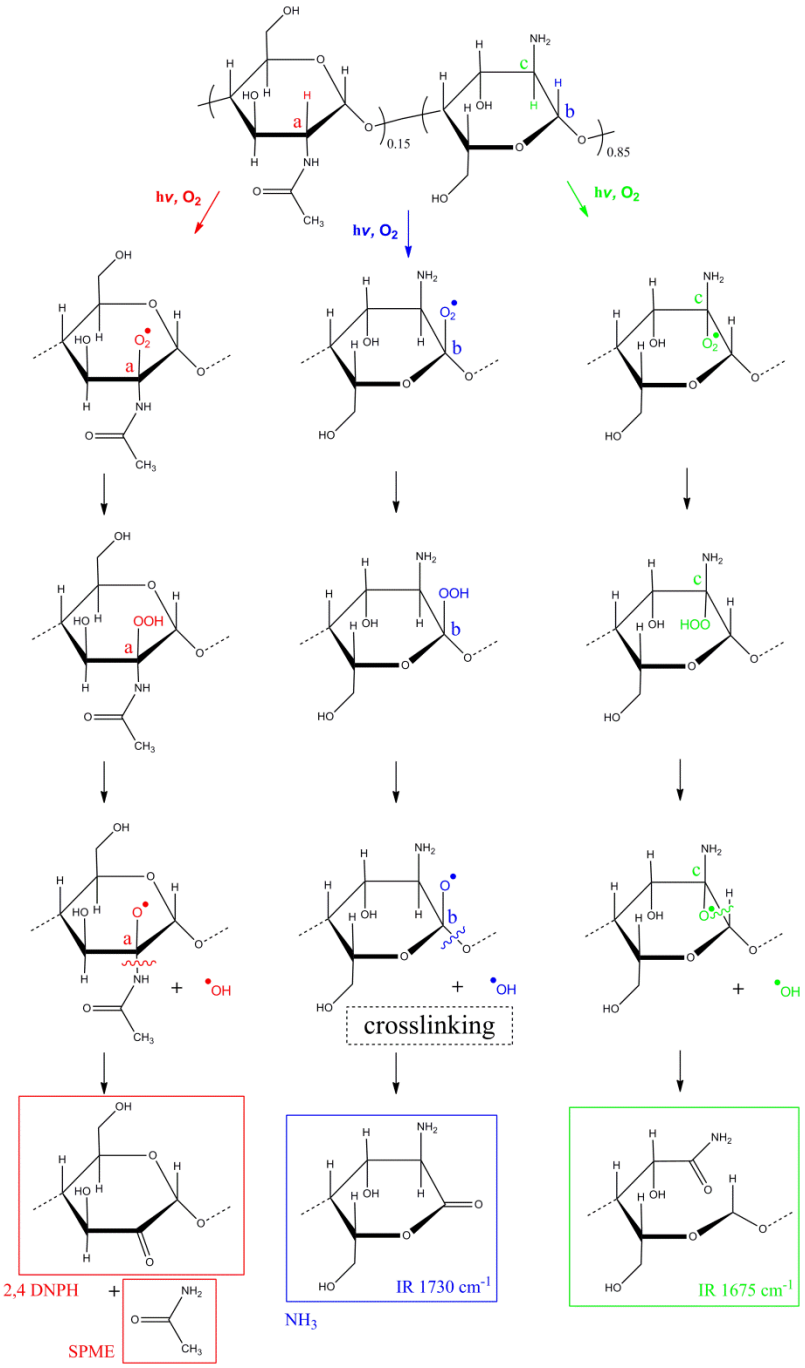

Scheme 2: Simplified photooxidation mechanism of chitosan

3.4 Consequences of photooxidation on the properties of chitosan

3.4.1 UV-visible analysis

Analysis of a chitosan film by UV-visible spectroscopy was carried out during photooxidation (Figure 4).

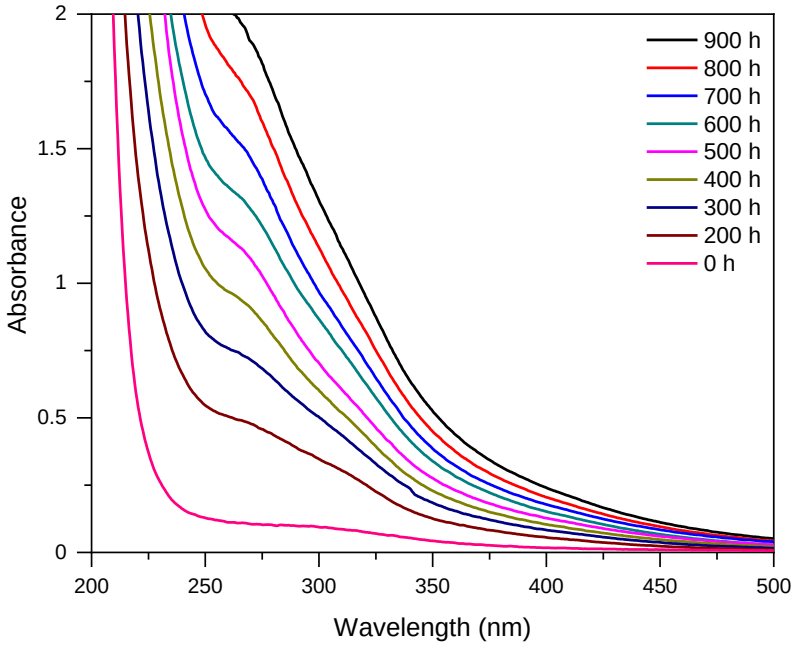

Figure 4: UV-Visible spectra of chitosan films during photooxidation (e = 25 µm)

The absorption front of the UV-vis spectra progressively shifted towards longer wavelengths during photooxidation, leading to yellowing of the chitosan film, and a shoulder with an absorption maximum could be observed at 270 nm. This feature was attributed to the formation of carbonyl groups and the cleavage of glycosidic bonds by several authors (Synytsya et al., 2012) (Wang et al., 2005).

3.4.2 Mechanical properties

Variations in the mechanical properties at the surface of chitosan films during photooxidation were assessed by elasticity measurements at the nanoscale (Table 1). To confirm the behaviour at the nanoscale, the polymer surface was analysed by AFM nano-indentation measurements. The loading/unloading indentation curves were measured for two irradiation times (see Figure S5).

The distance or displacement to reach the maximum force decreased after 200 h of irradiation. This is characteristic of an increase in the surface nano-hardness and Young's modulus. The increase in the nano-hardness of chitosan observed under irradiation can be correlated to crosslinking reactions.

One can also notice a small negative deflection after 200 h of irradiation that is consistent with the increase in the adhesion work. The increase in the adhesion work with the exposure time has already been connected (Bussiere, Rivaton, Therias & Gardette, 2012) to the accumulation of polar species at the surface of the sample and thus to the formation of oxidation products. In addition, the nano-hardness of the polymer sample can be calculated from these loading-unloading curves.

AFM nanoscale thermal analysis

In addition, variation in the glass transition temperature resulting from UV light exposure were monitored by AFM thermal analysis (Vita). The deflection-temperature curves (Figure S6) after 100 h and 300 h of irradiation were compared with the deflection-temperature curve before exposure. Nano-T_g values are reported in Table 1. After irradiation, the deflection shifts to higher temperatures. As T_g is related to the deflection, this result indicates that T_g increased with irradiation time. The Flory theory (Fox & Flory,1950) relates T_g to the molecular weight, reflecting crosslinking reactions.

Table 1: Evolution of nano-hardness (nano-Hv) and nano-T_g as a function of irradiation time.

Irradiation time	Nano-Hv (at 160 nm)	Nano-T_g (K)
0 h	90 ± 8 MPa	430 ± 5
100 h	150 ± 15 MPa	465 ± 5
200 h	230 ± 25 MPa	495 ± 10
300 h	280 ± 25 MPa	510 ± 5
400 h	330 ± 45 MPa	530 ± 15

The increase in nano-hardness and nano-T_g are consistent with crosslinking reactions leading to higher molecular weights, with a marked increase in the gel fraction (chitosan that became almost insoluble after 400 h of irradiation at $\lambda > 300$ nm in the presence of oxygen).

3.4.3 Surface properties

Roughness values (RMS) of a chitosan film surface were calculated before and after irradiation. Modifications of the roughness (RMS) displayed in Figure 5 show that RMS increased during irradiation.

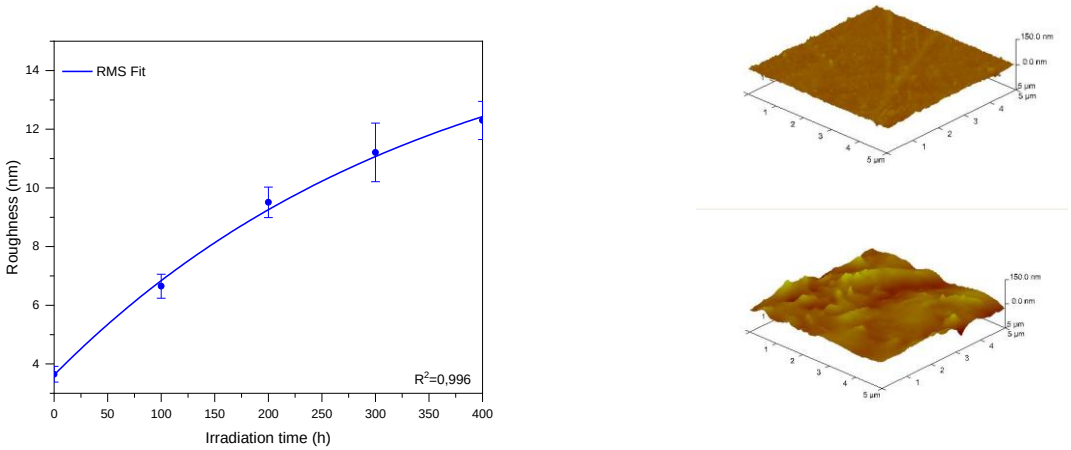

Figure 5: a) Change in roughness (■) versus irradiation time (line is obtained by an exponential fit).
b) Image of the chitosan film surface before and after 300 hours of irradiation.

As previously reported, these variations arise from the formation of oxidation products of the polymer sample and of volatile products (Berthumeyrie, Collin, Bussiere & Therias, 2014).

3.5 Multiscale correlation

As shown above, the degradation of chitosan provoked by exposure to UV light in the presence of air led to variations in the following:

- chemical structure (oxidation, chain scission/crosslinking)
- macromolecular architecture (increase in network density, i.e., T_g)
- mechanical properties (increase in hardness)
- surface properties (increase in roughness and yellowing).

Therefore, the degradation caused by exposure to UV light can be characterized by the following parameters: amide and gluconolactone formation, C-O-C conversion rate, tanδ, nano-indentation and increased hardness. To check the inter-connection between the evolutions of these parameters during irradiation, a quantitative description was attempted.

Figure 6 shows the variations in the concentrations of amide groups (IR band at 1675 cm^{-1}), gluconolactone (IR band at 1730 cm^{-1}), and ethers (IR band at 1150 cm^{-1}) during irradiation (the film thickness was 25 microns, and the absorption coefficients were as follows: CONH: 340-380 $L.mol^{-1}.cm^{-1}$, gluconolactone: 650-700 $L.mol^{-1}.cm^{-1}$, COC: 40-50 $L.mol^{-1}.cm^{-1}$) (from the literature) [Okamba-Diogo et al., 2014].

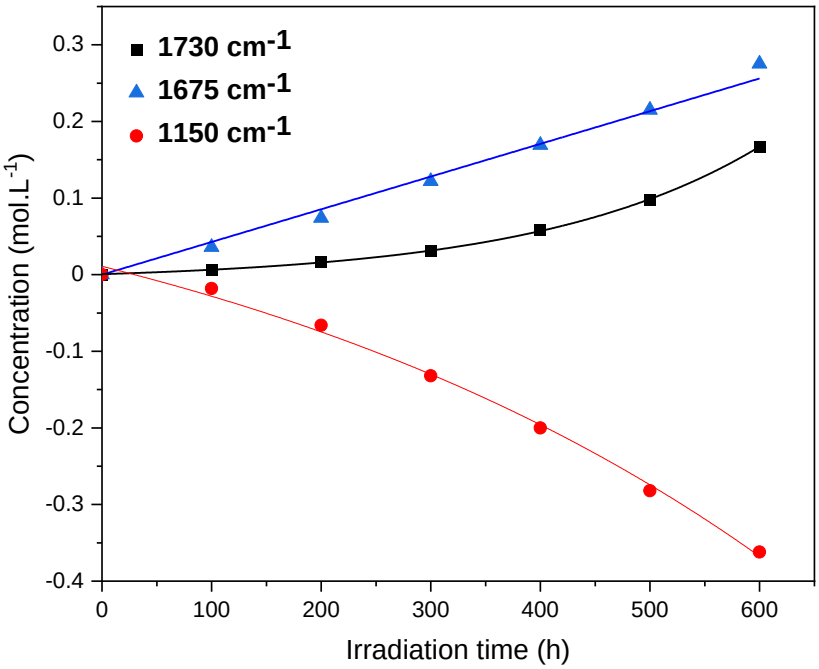

Figure 6: Concentration of the oxidation products (detected at 1675 cm^{-1} and at 1730 cm^{-1} in IR spectra) and disappearance of the C-O-C bond (detected at 1150 cm^{-1} in IR spectra) versus irradiation time.

Figure 6 shows that the concentration of amide groups (1675 cm^{-1}) produced during photooxidation was higher than the concentration of gluconolactone (1730 cm^{-1}). Indeed, the concentration of gluconolactone generated after 600 hours of ageing corresponded to the concentration of amide group after 100 hours of ageing.

To connect all the degradation criteria from the molecular scale to the macroscopic scale, we aimed to find kinetic information from the different parameters responsible for the degradation versus exposure time. We used a phenomenological model (Rose, Le Bras Bourbigot & Delobel, 1994) (Musto, Ragosta, Abbate & Scarinzi, 2008) to describe the kinetic processes of degradation as follows:

$$\frac{X(t)}{X(t=0)} = 1 - kt$$

$$X(t) = X(t=0).\exp(-kt)$$

where X(t) is the value of a selected parameter obtained for various times t, X (t=0) is the parameter value at t = 0 and k is the Arrhenius-type kinetic constant. The equation was applied to the experimental parameters X, such the absorbance A at 1730 cm^{-1}, nano-hardness, and T_g.

Table 2: Degradation rate (k) for the main degradation criteria of photooxidation

Parameters	**Kinetic model**	**k** ($h^{-1}.10^{-3}$)	**standard error** ($h^{-1}.10^{-3}$)	**C.coeff** χ^2
α C=O (1675 cm^{-1})	$\frac{A(t)}{A(t=0)} = 1 - kt$	0.475	0.05	0.999
Yellowing (A 400 nm)	$\frac{A(t)}{A(t=0)} = 1 - kt$	0.475	0.07	0.989
α C=O (1730 cm^{-1})	$A(t) = A(t=0).\exp(-kt)$	2.8	0.1	0.996
α COC	$A(t) = A(t=0).\exp(-kt)$	1.6	0.1	0.995
nano-Hardness/ Hardness	$A(t) = A(t=0).\exp(-kt)$	1.7	0.2	0.992
nano-Tg	$A(t)$	2.5	0.1	0.98
Roughness	$A(t)$	2.8	0.15	0.996

The results in Table 2 indicate that only the appearance of amide groups and the increase in yellowing follow zero-order kinetics. The accumulation of gluconolactone and the various parameters that were selected in an attempt to establish a correlation between the variation in chemical structure and mechanical properties follow a first-order kinetic, and the k values for the main parameters are similar (the average k value was $2.10^{-3}.h^{-1}$). The half-life time was calculated from the kinetics, and the average $t_{1/2}$ value was approximately 200 hours. The good agreement between the degradation-rate k-values of the different criteria confirms the cross-correlation established. These results underline the difference in reactivity of all the detected degradation species and confirm diverse routes of degradation.

4. Conclusion

Photooxidation of chitosan resulted in yellowing, crack formations, and an increase in roughness. The increases in network density and nano-hardness are relevant in terms of a reduction in the material's functional properties. A mechanism accounting for the main degradation routes for chitosan photooxidation at the molecular scale was proposed. We demonstrated the consequences of the chemical modifications on the material properties, and we showed correlations between these chemical modifications and the evolution of the mechanical properties. Our results allowed a « quantitative » correlation between the relevant degradation criteria.

Declaration of Interest

None

Figure captions

Figure 1: IR spectra of chitosan films (e = 25 µm) before and after 24 h Soxhlet extraction in MeOH (domain 1800-1000 cm^{-1}) and the chitosan powder in KBr pellets.

Figure 2: a) IR spectra of chitosan film (e = 25 µm) during photooxidation,
b) Subtracted IR spectra in carbonyl domain.

Figure 3: a) IR spectrum of a film (e = 25 µm) of chitosan blended with gluconolactone.
b) UV-visible spectra of a 600h photooxidized chitosan film before and after treatment with 2,4-DNPH.

Figure 4: UV-Visible spectra of chitosan film during photooxidation (e = 25 µm).

Figure 5: a) Change in roughness (■) versus irradiation time (line is obtained by an exponential fit).
b) Image of the chitosan film surface before and after 300 hours of irradiation.

Figure 6: Concentration of the oxidation products (detected at 1675 cm^{-1} and at 1730 cm^{-1} in IR spectra) and loss of the C-O-C bond (detected at 1150 cm^{-1} in IR spectra) versus irradiation time.

Table 1: Evolution of nano-hardness (nano-Hv) and nano-T_g as a function of irradiation time
Table 2: Degradation rate (k) for the main degradation criteria of photooxidation

Scheme 1: Chemical structure of chitosan
Scheme 2: Simplified photooxidation mechanism of chitosan

References

Abdelghany, A.M., Ayaad, D.M., Aboelkheir, A.M. (2019) The effects of prolonged UV irradiation on the physicochemical characteristics of chitosan lamellar films modified with nanoparticulate silver vanadate nanorods. *Polymer Bulletin, doi :10.1007/s00289-019-03029-x.*

Aider, M. (2010) Chitosan application for active bio-based films production and potential in the food industry: review, LWT – *Food science and Technology, 43*, 837-842.

Andrady, A.L., Torikai, A., Kobatake, T. (1996) Spectral Sensitivity of chitosan photodegradation. *Journal of Applied Polymer Science*, *62*, 1465-1471.

Berthumeyrie, S., Collin, S., Bussiere P.O., & Therias, S. (2014) Photooxidation of cellulose nitrate: new insights into degradation mechanisms. *Journal of Hazardous Material, 272*, 137-147.

Bussiere, P.-O., Rivaton, A., Therias, S., Gardette, J.-L. (2012) Multiscale Investigation of the Poly(N-vinylcarbazole) Photoageing Mechanism. *The Journal of Physical Chemistry B , 116*, 802-812.

Collin, S., Bussiere, P.O., Therias, S., Lambert, J.M., Perdereau, J, Gardette J.L. (2012) Physicochemical and mechanical impacts of photo-ageing on bisphenol a polycarbonate. *Polymer Degradation and Stability, 97*, 2284-2293.

Fox, T. G., Flory, P. J. (1950) Second Order Transition Temperatures and Related Properties of Polystyrene. I. Influence of Molecular Weight. *Journal of Applied Physics*, *21*, 581-591.

Gamiz-Gonzalez, M.A., Correia, D.M., Lanceros-Mendes, S., Sencadas, V., Gomez Ribelles, J.L., Vidaurre, A. (2017) Kinetic study of thermal degradation of chitosan as a function of deacetylation degree. *Carbohydrate Polymers, 167*, 52-58.

Gaume, J., Wong-Wah-Chung, P., Rivaton, A., Therias, S., Gardette, JL., (2011) Photochemical behavior of PVA as an oxygen-barrier polymer for solar cell encapsulation. *RSC Adv*ances, *1*, 1471-1481.DOI: 10.1039/C1RA00350J.

Huang, Y., Wu, Y., Huang, W., Yang, F., Ren, X. (2013) Degradation of chitosan by hydrodynamic cavitation. *Polymer Degradation and Stability, 98(1)*, 37-43.

Kasaai, M.R. (2008) A review of several reported procedures to determine the degree of N-acetylation for chitin and chitosan using infrared spectroscopy. *Carbohydrate Polymers, 71,* 497-508.

Kowalonek, J., (2017) Surface and thermal properties of UV-irradiated chitosan/poly(ethylene oxide) blends. *Journal of Photochemistry and Photobiology, A : Chemistry, 348,* 209-218.

Lien, C.F., Molnar, E., Toman, P., Tsibouklis, J., Pilkington, G.J., Gorecki, D.C., E. Barbu, E. (2012) In Vitro Assessment of Alkylglyceryl-Functionalized Chitosan nanoparticles as permeating vectors for the blood – brain barrier, *Biomacromolecules*, *13,* 1067-1073.

Moczek, L. & Nowakowska, M. (2007). Novel water-soluble photosensitizers from chitosan. *Biomacromolecules, 8*, 433-438.

Moore, R.F. (1963) The photochemical degradation of polyamides and related model *N*-alkylamides. *Polymer 4*: 493-513)

Mucha, M. &Pawlak, A. (2002) Complex study on chitosan degradability. *Polimery, 47* (7-8), 509-516.

Musto, P., Ragosta, G., Abbate, M., Scarinzi, G. (2008) Photo-oxidation of high performance epoxy networks: Correlation between the molecular mechanisms of degradation and the viscoelastic and mechanical response. *Macromolecules*, *41*, 5729-5743.

Nawi, M.A., Jawad, A.H., Sabar, S. ; Wan Ngah W.S. (2011) Photocatalytic-oxidation of solid state chitosan by immobilized bilayer assembly of TiO2-chitosan under a compact household flurescent lamp irradiation. *Carbohydrate Polymers*, *83*, 1146-1152.

Nazeer M.A., Yilgor, E., Yilgor, I. (2017) Intercalated chitosan/hydroxyapatite nanocomposites : Promising materials for bone tissue engineering applications. *Carbohydrate Polymers*, 17538-17546.

Ogawa, K., Yui, T., Okuyama, K. (2004). Three D structures of chitosan. *International Journal of Biological Macromolecules*, *34*, 1-8.

Okamba-Diogo, O., Richaud, E., Verdu, J., Fernagut, F., Guilment, J, Fayolle, B., (2014). Molecular and macromolecular structure changes in polyamide 11 during thermal oxidation, *Polymer Degradation and Stability, 108*, 123-132.

561 Oliver, W.C., Pharr, G.M. (1992) An improved technique for determining hardness and
562 elastic modulus using load and displacement sensing indentation experiments. *Journal of*
563 *Materials Research, 7* , 1564-1583.

564 Philippart, J.L., Sinturel, C., Gardette, J.L. (1997). Influence of light intensity on the
565 photooxidation of polypropylene.*Polymer Degradation and Stability, 58 (3),* 261-268.

566 Rideal, E.K. & J. S. Mitchell, J.S. (1937) Photochemical reactions in monolayers I-
567 Photochemical properties of the ketoimino linkage. *Proc. Roy. Soc.* (London), *159*, 206.

568 Rinaudo, M., Pavlov, G., J. Desbrieres, J. (1999) Influence of acetic acid concentration on the
569 solubilization of chitosan. *Polymer, 40*, 7029-7032.

570 Rose, N., Le Bras, M., Bourbigot, S., Delobel, R. (1994) Thermal oxidative degradation of
571 epoxy resins: evaluation of their heat resistance using invariant kinetic parameters. *Polymer*
572 *Degradation and Stability, 45*, 387-397.

573 Scott, G. (1995) Initiation processes in polymer degradation. *Polymer Degradation and*
574 *Stability, 48 (3),* 315-324.

575 Sharkey, W.H. & Mochel, W.E. (1959) Mechanism of the Photooxidation of Amides. *J. Am.*
576 *Chem. Soc. (8-12),* 3000-3005.

577 Sionkowska, A., Wisniewski, M., Skopinska, J., Vicini, S., Marsano, E. (2005) The influence
578 of UV irradiation on the mechanical properties of chitosan/poly(vinyl pyrrolidone) blends.
579 *Polymer Degradation and Stability, 88 (2)* , 261-267.

580 Sionkowska, A., Kazmarek, H., Wisniewski, M., Skopinska, J., Lazare, S., Tokarev, V.
581 (2006). The influence of UV irradiation on the surface of chitosan films. *Surface Science,*
582 *600*, 3775-3779.

583 Sionkowska, A., Skopinska-Wisniewska, J., Planecka, A., Kozlowska, J. (2010) The
584 influence of UV irradiation on the properties of chitosan films containing keratin. *Polymer*
585 *Degradation and Stability, 95(12),* 2486-2491.

586 Sionkowska, A., Planecka, A., Kozlowska, J., Skopinska-Wisniewska, J., Los, P. (2011)
587 Weathering of chitosan films in the presence of low- and high- molecular weight additives,
588 *Carbohydrate Polymers, 84*, 900-906.

589 Sionkowska, A., Planecka, A., Lewandowska, K., Kaczmarek, B., Szarszewska, P. (2013).
590 Influence of UV-irradiation on molecular weight of chitosan, *Progress on Chemistry and*
591 *Application of Chitin and Its derivatives, 18*, 21-28.

Sionkowska, A., Planecka, A., Lewandowska, K ., Michalska, M. (2014) The influence of UV-irradiation on thermal and mechanical properties of chitosan and silk fibroin mixtures. *Journal of Photochemistry and Photobiology, B : Biology, 140*, 301-305.

Sionkowska, A., Kaczmarek, B., Gnatowska, M., Kowalonek, J. (2015) The influence of UV-irradiation on chitosan modified by the tannic acid addition. *Journal of Photochemistry and Photobiology, B : Biology, 148, 333-339.*

Synytsya, A., Grafova, M., Slepicka, P., Gedeon, O., Synytsya, A. (2012). Modification of Chitosan-Methylcellulose composite films with meso-Tetrakis(4-sulfonatophenyl)porphyrin. *Biomacromolecules, 13(2),* 489-498.

Taskn, P., Cansag, H., Sen, M. (2014) The effect of degree of deacetylation on the radiation induced degradation of chitosan. *Radiation Physics and Chemistry, 94*, 236-239.

Tchemtchoua, V.T., Atanasova, G., Aqil, A., Filee, P., Garbacki, N., Vanhooteghem, O., Deroanne, C., Noël, A., Jerome, C., B. Nusgens, B. (2011) Development of a chitosan nanofibrillar scaffold for skin repair and regeneration, *Biomacromolecules, 12(9),* 3194-3204.

Valentin, R., Bonelli, B., Garrone, E., Di Renzo, F., Quignard, F. (2007) Accessability of the Functional Groups of Chitosan aerogel probed by FT-IR monitored deuteration. *Biomacromolecules, 8*, 3646-3650.

Villar-Chavero, M.M., Dominguez, J.C., Alonso, M.V., Oliet, M., Rodriguez, F. (2018) Thermal and kinetics of the degradation of chitosan with different deacetylation degrees under oxidizing atmosphere. *Thermochimica Acta, 670*, 18-26.

Wang, S-M., Huang, Q-Z., Wang, Q-S. (2005) Study on the synergetic degradation of chitosan with ultraviolet light and hydrogen peroxide. *Carbohydrate research 340(6),* 1143-1147.

Wasikiewicz, J.M., Yoshii, F., Nagasawa, N., Wach, R.A., Mitomo, H. (2005) Degradation of chitosan and sodium alginate by gamma radiation, sonochemical and ultraviolet methods. *Radiation Physics and Chemistry, 73(5),* 287-295. DOI: 10.1016/j.radphyschem.2004.09.021

Wasikiewicz, J.M., Yeates, S.G., (2013) « Green » molecular weight degradation of chitosan using microwave irradiation. *Polymer Degradation and Stability, 98(4),* 863-867.

Wilhelm, C. & Gardette, J.L. (1994) Infrared identification of carboxylic acids formed in polymer photooxidation. *Journal of Applied Polymer Science, 51(8),* 1411-1420.

622 Zawadzki, J. & Kaczmarek, H. (2010) Thermal treatment of chitosan in various conditions.
623 *Carbohydrate Polymers, 80*, 394-400.